Characterization of the structural, electronic and tribological properties of metal dichalcogenides by scanning probe microscopies

Charles M. Lieber and Yun Kim
Department of Chemistry, Harvard University, Cambridge, MA 02138 (U.S.A.)

Abstract

Scanning tunneling microscopy (STM) and atomic force microscopy (AFM) have been used to characterize the structural and electronic properties of single-crystal MoS_2, nickel-substituted MoS_2 ($Ni_xMo_{1-x}S_2$), and chalcogenide-substituted MoS_2 ($MoS_{2-x}Ch_x$, Ch ≡ Se, Te) at the atomic level. Images of $Ni_{0.1}Mo_{0.9}S_2$ demonstrate that nickel substitution causes localized changes in the electronic states, although the structure of the surface sulfur layer is unchanged compared with MoS_2. Investigations of $MoS_{1.75}Se_{0.25}$ also show that within the detection limits of AFM selenium substitution does not perturb the sulfur surface structure, and STM data further indicate that the substituted selenium is electronically delocalized. In contrast, AFM studies of $MoS_{1.75}Te_{0.25}$ show that tellurium substitution produces atomic-sized structural protrusions that may modify significantly the tribological properties of MoS_2. In addition, we demonstrate that material wear can be characterized on an atomic scale by AFM. These studies indicate that the microscopic origin of material wear as well as the local structure and electronic properties should be considered to develop further models of friction and wear in metal dichalcogenide materials.

1. Introduction

Molybdenum disulfide (MoS_2) has been one of the most widely studied solid state lubricants [1–8]. The useful tribological properties of MoS_2 have typically been rationalized in terms of the unique quasi-two-dimensional layered structure of this solid (Fig. 1) [1]. This structure consists of covalently bonded three-atom S–Mo–S layers that are held together primarily by van der Waal's forces [9, 10]. The very weak interlayer bonding gives rise to a small layer–layer shear energy, and hence layer–layer sliding friction is low. Interestingly, MoS_2 has the best lubricating properties of any of the transition metal dichalcogenides even though many of these materials are isostructural. It has thus been apparent that properties in addition to the layered structure must cause the different tribological properties observed experimentally in the metal dichalcogenides. Several studies suggest that differences in the electronic structure of the transition metal, for example, d^2-Mo *vs.* d^1-Nb, can explain observed variations in friction for structurally similar materials [3, 4]. These qualitative structural and electronic ideas can be used to explain macroscopic friction in the metal dichalcogenide materials; however, a detailed microscopic picture that relates atomic level structural, electronic, and tribological properties to macroscopic wear and friction has yet to be developed. It is essential, however, to develop such a microscopic model since it would enable the rational design and development of modified or new materials that have improved lubrication properties compared with MoS_2.

To develop a more detailed understanding of MoS_2 and other metal dichalcogenide materials we have been using scanning tunneling microscopy (STM) and atomic force microscopy (AFM) [11–13]. STM and AFM can provide direct atomic resolution data that address the structural, electronic, wear, and frictional properties of interfaces [11–16], and herein we report studies of single-crystal MoS_2, $Ni_xMo_{1-x}S_2$, $MoS_{2-x}Se_x$, and $MoS_{2-x}Te_x$. These investigations address at the atomic level the structural and electronic properties of MoS_2 and how these properties vary on metal (nickel) and anion (selenium, tellurium) substitution. In addition, we have carried out preliminary studies of atomic-scale wear in the metal dichalcogenide materials.

2. Experimental details

Single crystals of MoS_2, $Ni_{0.1}Mo_{0.9}S_2$, $MoS_{2-x}Se_x$ ($x = 0.25, 0.5$) and $MoS_{1.75}Te_{0.25}$ were grown from polycrystalline powders by chemical vapor transport [17–19]. Briefly, a stoichiometric mixture (5 g total mass) of molybdenum and sulfur was sealed in a quartz tube under vacuum and reacted for 10 days at 1000 °C. Following reaction, the polycrystalline powder was ground and resealed under vacuum in a quartz tube together with excess sulfur (60 mg) and iodine (100 mg). Crystals were grown in a 50–100 °C gradient

0040-6090/91/$3.50

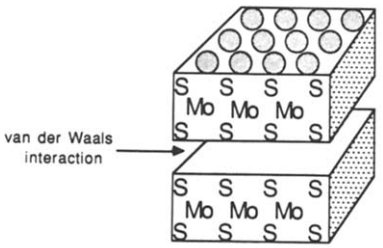

Fig. 1. Schematic diagram of MoS_2 illustrating the two S–Mo–S layers. These layers are held together by van der Waals' forces.

over a three week period. The crystals obtained from the growth region had the expected plate-like layered morphology and varied in size from 1 mm × 1 mm to 3 mm × 3 mm. The metal- and chalcogenide-doped materials were grown using similar conditions. Elemental analyses (XPS, AES and atomic absorption spectroscopy) showed that the metal and chalcogenide substituted crystals were stoichiometric.

The scanning tunneling and atomic force microscopes used in these studies were commercial instruments (Nanoscope, Digital Instruments, Inc.). STM images were recorded in the constant current mode with platinum–iridium (80%–20%) alloy tips that were mechanically formed. The AFM images were recorded in the constant force mode with microfabricated cantilevers. A laser–position sensitive detector system was used to determine motion of the cantilever. Experiments were carried out on freshly cleaved crystal surfaces in air and in an argon-filled inert atmosphere glove-box equipped with a purification system for the removal of water and oxygen; the atomic resolution data obtained in both environments were similar. The calibration of the piezotube scanner and the analysis of the digital image data have been described previously [11–13].

3. Results and discussion

STM and AFM gray scale images of cleaved MoS_2 single crystals are shown in Fig. 2. In these images light corresponds to raised surface features and dark to depressions. The STM image of MoS_2 exhibits a hexagonal lattice with a period of 0.31 ± 0.01 nm. This lattice constant is consistent with the sulfur–sulfur lattice spacing determined by crystallography and is similar to previously reported STM results for MoS_2 [20, 21]. AFM images of MoS_2 crystals also exhibit a hexagonal structure with a period of 0.32 ± 0.01 nm. The AFM and STM results thus yield a similar picture for the surface structure of MoS_2. Furthermore, these data serve as a reference with which the STM and AFM studies of the substituted MoS_2 materials discussed below can be compared.

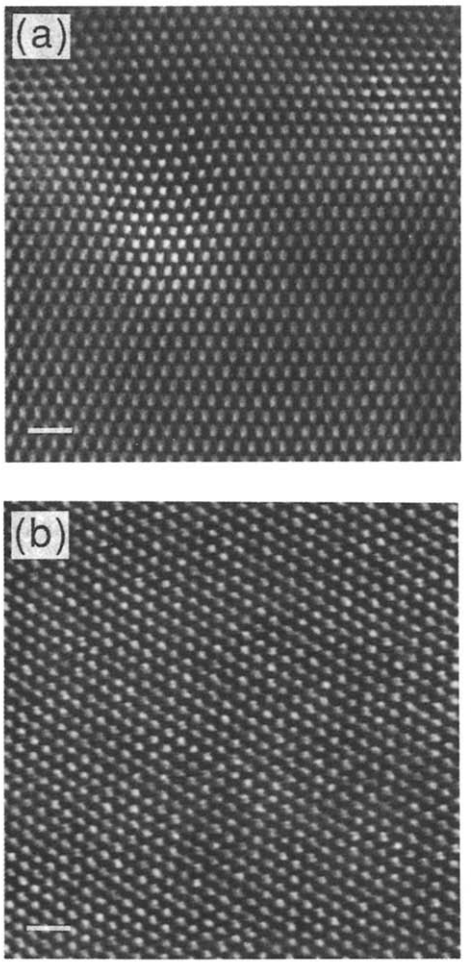

Fig. 2. 9 nm × 9 nm images of MoS_2. The (a) STM and (b) AFM data are unfiltered. The white scale bar corresponds to 0.9 nm.

We have used STM and AFM to characterize for the first time the local structural and electronic properties of $Ni_xMo_{1-x}S_2$ single crystals. These nickel-substituted materials are a particularly attractive system for high resolution studies since recent work has shown that nickel-containing MoS_2 thin films have enhanced tribological properties compared with pure MoS_2 films [22, 23]. The structures of the single-crystal $x = 0$–0.1 materials determined by single-crystal X-ray diffraction are the same as that of MoS_2 and, therefore, it is apparent that nickel substitution does not change the average structural properties of MoS_2 crystals. Typical atomic resolution STM and AFM images of cleaved $Ni_{0.1}Mo_{0.9}S_2$ crystals are shown in Fig. 3. The AFM image, which reflects primarily surface structure, exhibits a regular atomic lattice with a period of 0.31 ± 0.01 nm. This structure corresponds to the surface sulfur atoms and is similar to the surface structure of MoS_2 determined by AFM. Careful analysis of the vertical corrugation of the sulfur atoms determined from the AFM images of $Ni_{0.1}Mo_{0.9}S_2$ shows that there

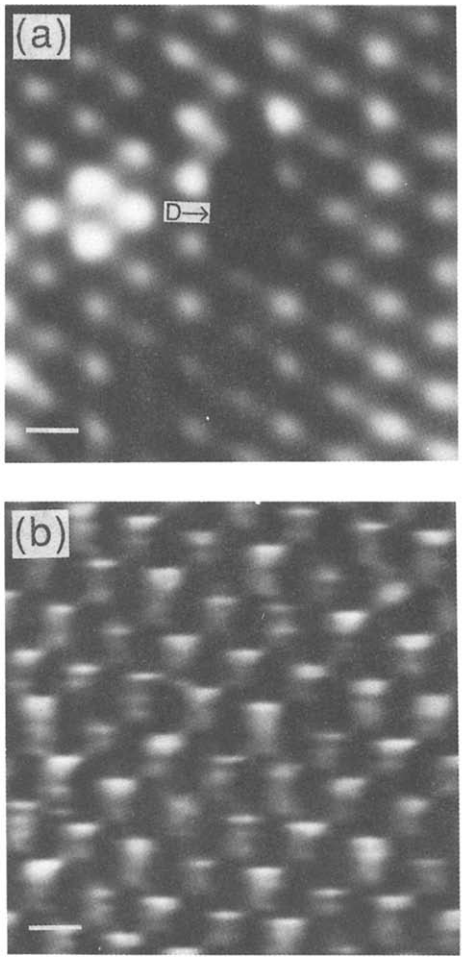

Fig. 3. 2.5 nm × 2.5 nm images of $Ni_{0.1}Mo_{0.9}S_2$. (a) The STM data have been filtered to remove high frequency noise; (b) the AFM image is unfiltered. The defect in the STM image is marked with a "D". The white scale bar corresponds to 0.3 nm.

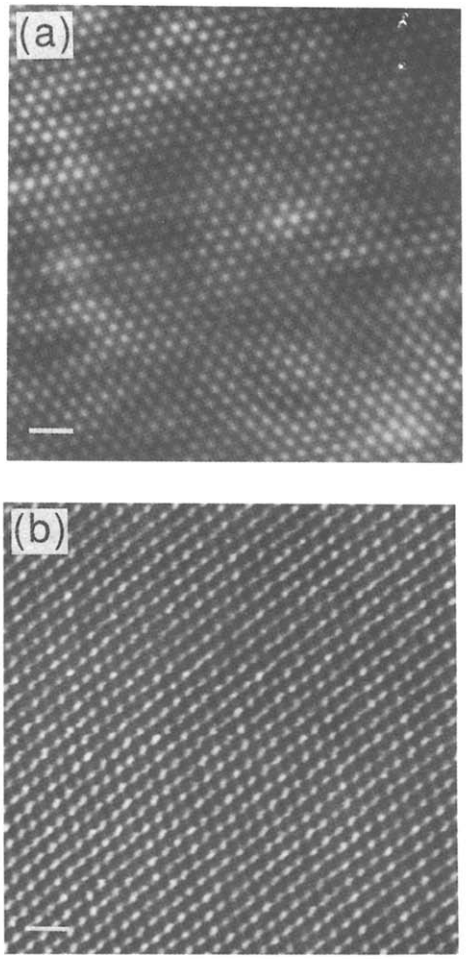

Fig. 4. 9 nm × 9 nm (a) STM and (b) AFM images of $MoS_{1.75}Se_{0.25}$. The selenium does not perturb the surface structure significantly in these materials. The white scale bar corresponds to 0.9 nm.

are peak-to-peak variations in the sulfur corrugation for the nickel-substituted material that may reflect differences in Ni–S *vs.* Mo–S bonding. Small peak-to-peak corrugation variations are, however, also observed in pure MoS_2 and thus additional studies will be needed to confirm this point.

In contrast to these AFM results, STM images of $Ni_{0.1}Mo_{0.9}S_2$ exhibit pronounced defects (D) in the hexagonal atomic lattice (Fig. 3(a)). These defects correspond to regions containing several surface atomic sites that have a corrugation 50%–70% lower than the surrounding lattice. Since the AFM data conclusively show that there are no large structural variations due to nickel substitution these defects can be attributed to a variation in the density of electronic states due to nickel in the lattice [24–26]. Hence, we can conclude that on the atomic scale nickel substitution appears only to affect the electronic states near the Fermi level and not to perturb significantly the structure. Such localized electronic changes are not expected to enhance layer–layer sliding or material plasticity, and thus additional studies will be required to elucidate the microscopic origin of the reduced macroscopic coefficient of friction observed in nickel-containing MoS_2 thin films [22, 23].

To investigate further the structural and electronic effects of substitution in MoS_2 we have also investigated selenium- and tellurium-doped MoS_2. X-ray diffraction studies of $MoS_{1.75}Se_{0.25}$ and $MoS_{1.75}Te_{0.25}$ crystals have shown that the 2H-MoS_2 crystal structure is retained for this substitution level. The small systematic changes in lattice parameters with substitution further indicate that replacement of sulfur with selenium or tellurium is random. Atomic resolution STM and AFM images of $MoS_{1.75}Se_{0.25}$ exhibit a similar hexagonal lattice with a period of 0.32 ± 0.01 nm and 0.32 ± 0.01 nm respectively (Fig. 4). In addition, the observed atomic vertical corrugations in these STM and AFM images are similar to the corrugations determined

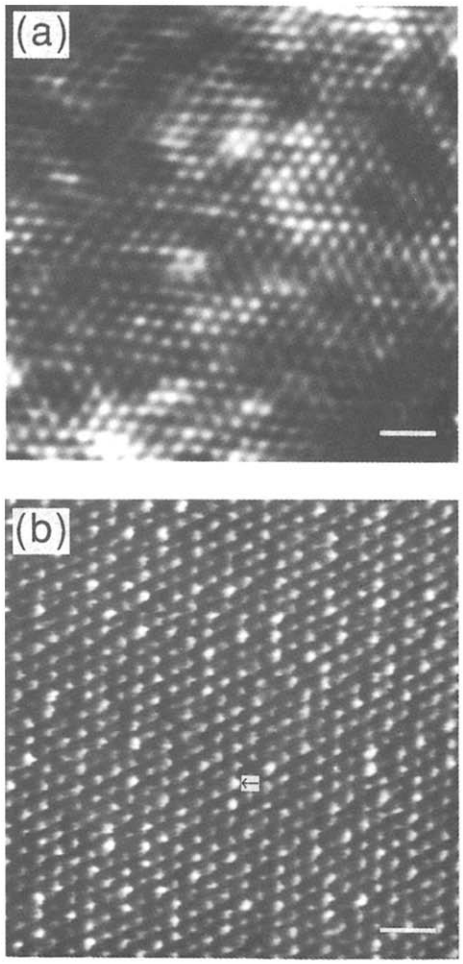

Fig. 5. 8 nm × 8 nm images of $MoS_{1.75}Te_{0.25}$. (a) The STM image has been filtered to remove high frequency noise; (b) however, the AFM image corresponds to raw data. The small arrow in (b) highlights one local atomic protrusion. The white scale bar corresponds to 1.0 nm.

from the images of MoS_2. These STM and AFM data show that the electronic and the structural properties of the MoS_2 crystal surface are not perturbed significantly by selenium substitution and, therefore, it is expected that the coefficient of friction for $MoS_{1.75}Se_{0.25}$ will be similar to that for MoS_2.

In contrast to the data for the selenium-containing materials, we observe significant atomic level structural changes at the surfaces of tellurium-substituted MoS_2. Typical images of $MoS_{1.75}Te_{0.25}$ are shown in Fig. 5. The STM image exhibits hexagonal structure with a period and vertical corrugation that is the same within experimental error as we determined for pure MoS_2. These results show that there are no large local perturbations in the electronic states in $MoS_{1.75}Te_{0.25}$, and thus we suggest that tellurium substitution is electronically delocalized. Unlike the STM data, AFM images show well-defined atomic size protrusions in the hexagonal lattice (Fig. 5(b)). The number of protrusions

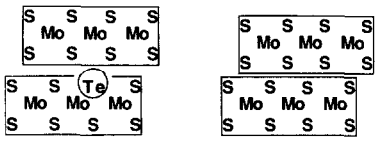

Fig. 6. Schematic view illustrating a possible structural manifestation of tellurium substitution based on the AFM data. In this model the tellurium sites reduce the layer–layer interaction relative to pure MoS_2.

scales directly with the concentration of tellurium in a series of $MoS_{2-x}Te_x$ materials, and thus we suggest that these features correspond to a direct observation of tellurium atoms in the lattice. It is possible that these localized structural features may reduce the layer–layer interaction in $MoS_{2-x}Te_x$ *vs.* MoS_2 as shown schematically in Fig. 6. An increase in layer–layer separation as indicated in Fig. 6 should occur at the relatively high concentrations of tellurium in our materials. Low tellurium concentrations could, however, inhibit shear due to localized lattice distortions. Hence, it will be important in the future to determine whether such structural protrusions affect the macroscopic coefficient of friction in these substituted materials.

Lastly, we have used AFM to study wear in the transition metal dichalcogenide materials at the atomic level. Previously, differences in macroscopic frictional properties of structurally similar transition metal dichalcogenides, such as MoS_2 and $NbSe_2$, have been attributed to variations in layer–layer sliding due to the distinct electronic structure of the metals (*e.g.* d^2-Mo *vs.* d^1-Nb) [3, 4]. To investigate the validity of such models further we have expanded our AFM studies to include measurements on $NbSe_2$. A series of AFM images recorded in the same spatial area as a function of time are shown in Fig. 7. It is readily apparent from these images that during the 9 min time interval between the acquisition of the two images $NbSe_2$ material is worn away from the surface by the AFM tip. No such material wear has, however, been observed on surfaces of MoS_2 imaged for a similar time period. These preliminary results show that atomic-scale wear on $NbSe_2$ and MoS_2 single crystals differs significantly, and we suggest that these differences may also play an important and as yet unrecognized role in determining differences in the tribological properties of the metal dichalcogenides.

4. Conclusions

In summary, we have used STM and AFM to characterize the structural and electronic properties of MoS_2 and nickel-, selenium-, and tellurium-substituted MoS_2 at the atomic level. Studies of $Ni_{0.1}Mo_{0.9}S_2$ have

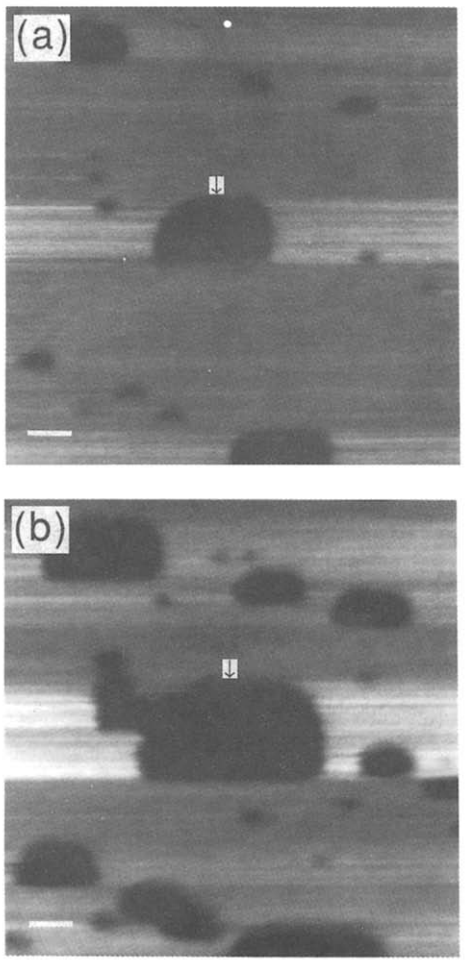

Fig. 7. 200 nm × 200 nm gray scale AFM images of $NbSe_2$ recorded in the same spatial location on the sample surface. The time interval between (a) and (b) was 9 min. Arrows highlight one 0.7 nm deep hole in the surface that becomes larger during this time interval. The data in these images are unfiltered. The white scale bar corresponds to 2.0 nm.

demonstrated that nickel substitution causes localized changes in the electronic states, although the structure of the surface sulfur layer is nearly unchanged compared with MoS_2. Investigations of $MoS_{1.75}Se_{0.25}$ have also shown that within the detection limits of AFM selenium substitution does not perturb the sulfur surface structure, and furthermore the STM data have indicated that the substituted selenium is electronically delocalized. In contrast, AFM studies of $MoS_{1.75}Te_{0.25}$ have shown that tellurium substitution produces atomic-sized structural protrusions that may modify significantly the tribological properties of MoS_2. In addition, we have demonstrated that material wear can be characterized on an atomic scale by AFM. These studies indicate that the microscopic origin of material wear as well as the local structural and electronic properties should be considered to develop further models of friction and wear in metal dichalcogenide materials.

Acknowledgments

We thank L. Burggraf and M. Donley for helpful discussions. C.M.L. acknowledges support of this work by the Air Force Office of Scientific Research and the David and Lucile Packard Foundation.

References

1 W. O. Winter, *Wear*, *10* (1967) 422.
2 W. E. Jamison, *ASLE Trans.*, *15* (1972) 296.
3 W. E. Jamison, *Proc. 3rd ASLE Int. Solid Lubrication Conf., Denver, CO*, in *ASLE SP-14*, 1984, p. 73 (American Society of Lubrication Engineers, New York).
4 P. D. Fleischauer, *Thin Solid Films*, *154* (1987) 309.
5 T. Spalvins, *J. Vac. Sci. Technol. A*, *5* (1987) 212.
6 E. W. Roberts, *Proc., Inst. Mech. Eng., London*, *1* (1987) 503.
7 J. K. G. Panitz, L. E. Pope, J. E. Lyons and D. J. Staley, *J. Vac. Sci. Technol. A*,*6* (1988) 1166.
8 M. R. Hilton and P. D. Fleischauer, *J. Mater. Res.*, *5* (1990) 406.
9 J. A. Wilson and A. D. Yoffe, *Adv. Phys.*, *18* (1969) 193.
10 A. A. Balchin, in F. Levy (ed.), *Crystallography and Crystal Chemistry of Materials with Layered Structures*, Vol. 2, Reidel, Boston, MA, 1976, p. 1.
11 X. L. Wu, P. Zhou and C. M. Lieber, *Phys. Rev. Lett.*, *61* (1988) 2604.
12 X. L. Wu and C. M. Lieber, *Science*, *243* (1989) 1703.
13 H. Chen, X. L. Wu and C. M. Lieber, *J. Am. Chem. Soc.*, *112* (1990) 3326.
14 C. M. Mate, G. M. McClelland, R. Erlandsson and S. Chiang, *Phys. Rev. Lett.*, *59* (1987) 1942.
15 E. Meyer, H. Heinzelmann, P. Grutter, Th. Jung, H.-R. Hidber, H. Rudin and H.-J. Guntherodt, *Thin Solid Films*, *181* (1989) 527.
16 W. Zhong and D. Tomanek, *Phys. Rev. Lett.*, *64* (1990) 3054.
17 A. A. Al-Hilli and B. L. Evans, *J. Cryst. Growth*, *15* (1972) 93.
18 R. M. A. Lieth and J. C. J. M. Terhell, in R. M. A. Lieth (ed.), *Preparation and Crystal Growth of Materials with Layered Structures*, Boston, MA, 1977, p. 141.
19 J. Baglio, E. Kamieniecki, N. DeCola, C. Struck, J. Marzik, K. Dwight and A. Wold, *J. Solid State Chem.*, *49* (1983) 166.
20 M. Weimer, J. Kramer, C. Bai and J. D. Baldeschwieler, *Phys. Rev. B*, *37* (1988) 4292.
21 D. Sarid, T. D. Henson, N. R. Armstrong and L. S. Bell, *Appl. Phys. Lett.*, *52* (1988) 2252.
22 B. C. Stupp, *Proc. 3rd ASLE Int. Solid Lubrication Conf., Park Ridge, IL*, in *ASLE SP-14*, 1984, p. 217 (American Society of Lubrication Engineers, New York).
23 B. C. Stupp, *Proc. Air Force Tribology Technical Review, Fairborn, OH, 1989*, in the press.
24 J. Tersoff and D. R. Hamann, *Phys. Rev. B*, *31* (1985) 805.
25 P. K. Hansma and J. Teroff, *J. Appl. Phys.*, *61* (1987) R1.
26 Y. Kuk, *Rev. Sci. Instrum.*, *60* (1989) 165.